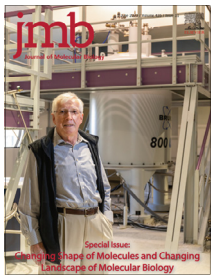

Impact on *S. aureus* and *E. coli* Membranes of Treatment with Chlorhexidine and Alcohol Solutions: Insights from Molecular Simulations and Nuclear Magnetic Resonance

Callum Waller [1,2], Jan K. Marzinek [2], Eilish McBurnie [1,2], Peter J. Bond [2,3*], Philip T. F. Williamson [4*] and Syma Khalid [1,5*]

*1 - **School of Chemistry,** University of Southampton, SO17 1BJ, UK*
*2 - **Bioinformatics Institute,** 30 Biopolis Street, Singapore 138671, Singapore*
*3 - **National University of Singapore,** 14 Science Drive 4, Singapore 117543, Singapore*
*4 - **School of Biological Sciences,** University of Southampton, SO17 1BJ, UK*
*5 - **Department of Biochemistry,** University of Oxford, OX1 3QU, UK*

Correspondence to Peter J. Bond, Philip T.F. Williamson and Syma Khalid: Bioinformatics Institute, 30 Biopolis Street, Singapore 138671, Singapore (Peter J. Bond); School of Chemistry, University of Southampton, SO17 1BJ, UK (Philip T.F. Williamson) and Department of Biochemistry, University of Oxford, OX1 3QU, UK (Syma Khalid).
syma.khalid@bioch.ox.ac.uk (S. Khalid) @ProfSyK (S. Khalid)
https://doi.org/10.1016/j.jmb.2023.167953
Edited by Sheena Radford

Abstract

Membranes form the first line of defence of bacteria against potentially harmful molecules in the surrounding environment. Understanding the protective properties of these membranes represents an important step towards development of targeted anti-bacterial agents such as sanitizers. Use of propanol, isopropanol and chlorhexidine can significantly decrease the threat imposed by bacteria in the face of growing anti-bacterial resistance *via* mechanisms that include membrane disruption. Here we have employed molecular dynamics simulations and nuclear magnetic resonance to explore the impact of chlorhexidine and alcohol on the *S. aureus* cell membrane, as well as the *E. coli* inner and outer membranes. We identify how sanitizer components partition into these bacterial membranes, and show that chlorhexidine is instrumental in this process.

Introduction

Pathogenic bacteria pose an enormous threat to human, animal, and plant health, especially given the rate at which resistance to current antibiotics is developing.[1–2] Effective methods of sanitization, such as antimicrobial hand and body scrubs, are essential in the control of widespread diseases as they offer a route to decreasing the rates of infection through human contact.[3–5] To develop new and more effective sanitizing agents, it is essential to understand their mechanisms of action against different bacterial membranes.

Chlorhexidine (CHX) is a member of a chemically related group of antimicrobials called bisbiguanides that form a di-cation at physiological pH (Figure 1).[6] The structure of CHX consists of two chlorophenyl (CPL) functional groups, each bonded to a separate biguanide (BGU) connected *via* a hexane (HEX) linker. Its structure and cationic charge are thought to be key to its bactericidal properties.[7] CHX is widely used as an antiseptic and disinfectant due to its broad efficacy, affordability, and safety, and it is commonly found in mouth washes and surgical scrubs.[8–9] It is effective against both Gram-positive and Gram-negative bacteria. CHX is thought to achieve bacterial cell death by binding

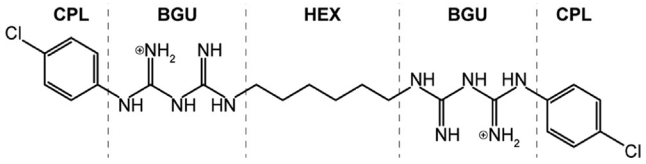

Figure 1. Separation of CHX into key functional groups which are necessary in the interaction of CHX with a PL membrane.

to the lipid bilayer headgroups and disrupting the membrane, leading to leakage of cellular contents. Hence, it is often combined with alcohol which is theorised to work in a similar way.[10] Under physiological pH the two BGU groups carry a cationic charge of 1 *e* each. The cationic nature of the molecules is proposed to play a major role in their interaction with negatively charged bacterial membranes.[11]

Short chain alcohol molecules are theorised to kill bacteria primarily by disrupting the membrane, similarly to CHX.[12] The value of topically applied alcohol as an antibacterial agent is well known, and has been proven as an effective form of defence against a plethora of pathogens *in vivo*, including *E. coli* and *S. aureus*.[3–5,13] This is largely attributed to macroscale perturbations which are imposed upon the bacterial cytoplasmic membrane, a model which was expanded upon by Feller et al.[14] who tracked the permeation of alcohol across a POPC membrane *via* nuclear Overhauser enhancement (NOE) spectroscopy.[15] This showed that alcohol accumulates mostly around the phosphate region of the phospholipid (PL) membrane, with the carbon chains of alcohol orientated toward the membrane centre. Further to this, it has been shown that the introduction of short-chained alcohols to a PL membrane can significantly affect the surface area per lipid (APL) and membrane thickness.[16] More recently this phenomenon was supported using molecular dynamics (MD) simulations by Ghorbani et al.[17] This also showed that following diffusion from the bulk ethanol solution there is very little diffusion of alcohol back out of the membrane plane.

CHX is theorised to bind at the headgroup region of membranes *via* the CPL and BGU functional groups as a 'wedge', parting the headgroups and creating gaps which make the membrane 'leaky'.[18] This charge interaction between the BGU region and the bilayer was shown by Oosten et al.[19] to result in binding further from the membrane centre but more strongly to the headgroup region in more negatively charged membranes. It has been demonstrated *via* cell culture experiments and verified by Franz diffusion cell studies that unlike other antiseptics, CHX can remain active due to epidermis binding even after the bulk of the sanitizer solution has been washed away.[20–21] CHX is active against *E. coli* (archetypal Gram-negative bacteria) and *S. aureus* (archetypal Gram-positive bacteria).[11] These two examples present three different kinds of membranes with alternative lipid compositions to CHX; the inner (EcIM) and outer membrane (EcOM) of *E. coli*, and the cell membrane of *S. aureus* (SaCM). CHX in sanitizing agents is available in both alcohol and aqueous solutions.

The EcOM contains lipopolysaccharide (LPS) in the outer leaflet and PLs in the inner leaflet, whereas the EcIM and SaCM contain PLs in both leaflets. The PLs in both the inner leaflet of the EcOM and both leaflets of the EcIM are phosphoethanolamine (PE), phosphoglycerol (PG) and cardiolipin (DPG) in a ratio of 90:5:5.[22] The precise details of the LPS chemical structure are dependent upon the *E. coli* strain. Briefly, the polar region of LPS is composed of layers of sugars, some of which are phosphorylated, whereas the hydrophobic portion typically has six hydrocarbon tails.[23–24] The SaCM is composed of PG, lysyl-phosphatidylglycerol (LPG) and DPG in a ratio of 54:36:10.[25–26] The main difference between the SaCM and the EcIM is the presence of LPG instead of PE, which provides the capacity for headgroup hydrogen bonding between LPG and PG while also lowering the overall membrane charge.[27]

To gain molecular insight into the mechanism(s) of action of CHX on the membranes of *E. coli* and *S. aureus*, here we have employed a combination of atomistic MD simulations and solid-state nuclear magnetic resonance (NMR) to study CHX in aqueous and alcohol solutions with the three membrane types presented by the two bacterial species. We present data detailing the partitioning of alcohol and chlorhexidine into bacterial membranes *via* a multidisciplinary approach, using MD and NMR in tandem to determine both their conformational and orientational properties. Our data helps to rationalize the origins of the characteristic membrane deformations generally associated with the use of alcohol and CHX as sanitising agents.

Results

Interaction between chlorhexidine and the bacterial membranes in aqueous solution

200 ns simulations were performed in triplicate where 0.5% w/v CHX in 0.15 M KCl was applied on either side of the three membranes (SaCM,

EcIM and EcOM). Visual inspection of the systems after 200 ns revealed little perturbation of the membranes in any of the simulations. The insertion depth was evaluated by calculating the CHX density in the z dimension (parallel to the membrane normal). Figure 2(a) shows greater penetration into the sub-headgroup region of the SaCM compared to either of the *E. coli* membranes. There was a shift in the CHX density towards the centre of the membrane as the simulation proceeds, while no such shift was observed for the *E. coli* membranes. The deeper penetration of CHX may be due to the higher negative charge in the headgroup region of the SaCM (−0.3 e per lipid), compared to the *E. coli* PL leaflets (−0.15 e per lipid) enabling stronger stabilising electrostatic interactions. This is in agreement with previously reported findings by

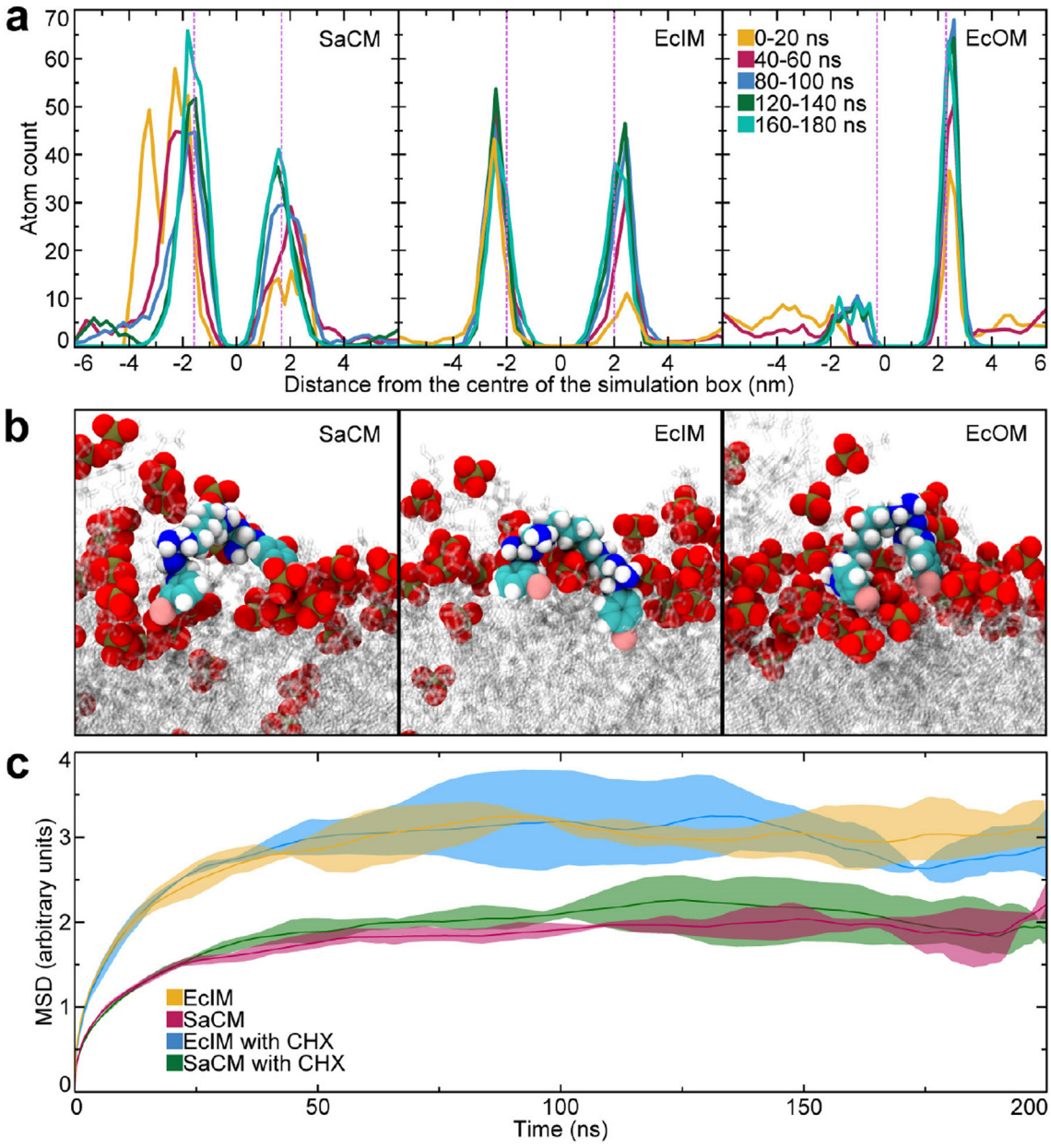

Figure 2. Analysis of the SaCM, EcIM and EcOM when exposed to 0.5 w/v CHX in a 0.15 M solution of KCl. (a) 20 ns block average density of CHX at 40 ns intervals along the z-axis of the simulation box for the entire 200 ns production run with average headgroup phosphate position as a pink, dotted line. (b) Snapshots of CHX C-shape binding in the SaCM, EcIM and EcOM systems are shown as spheres with phosphate oxygen in red, phosphate phosphorous in gold, carbon in cyan, nitrogen in blue, chlorine in pink, hydrogen in white and lipids as translucent. (c) Mean squared displacement (MSD) of lipids in the SaCM and EcIM with and without CHX analysed in the x and y dimensions (the membrane surface).

Van Oosten et al.[19] that CHX binds more strongly with increased charge disparity. There was no penetration into the sub-headgroup region of the LPS leaflet of the EcOM, despite the high charge of LPS. The slow-moving, almost impenetrable nature of LPS has been well-documented in both experimental and simulation studies.[28] For the PL membranes, over the course of 200 ns the CHX molecules transitioned from partial interaction with the membrane on one terminal BGU-CPL region, to mostly being intercalated and bound by both termini, as illustrated in Figure 2(b). In this configuration, the BGU and CPL functional groups are buried in/beneath the phosphate region toward the ester functional groups, while the HEX group lies along the bilayer surface. The interaction observed here has been termed as a 'c-shape' mode of binding and is reminiscent of the wedge proposed by Komljenović et al.[18] It should be noted, however, that the wedge they proposed is an inverted conformation, with the CPL-BGU region located in the lipid headgroups and the HEX functional group buried in the lipid tail region. The mean squared displacement (MSD) of lipids in the SaCM and EcIM when exposed to CHX was tracked in order to assess the effect of c-shape binding on lipid mobility (Figure 2(c)). Due to headgroup interactions between PG and LP in the SaCM the MSD was much lower. However, both membranes had a lower MSD after 200 ns of production simulation with CHX than they did without, especially in the case of EcIM, confirming previous findings.[29] In order to assess the stability of the c-shape conformation. The CPL-CPL distance of CHX in the SaCM and EcIM systems was measured. This showed significant fluctuations, but the average distance was approximately 13 Å after 200 ns of production in both the SaCM and EcIM systems (see Supplementary Figure 1). The solvent accessible surface area (SASA) of the CHX was calculated for the simulated trajectories to assess any potential clustering of CHX molecules, but this revealed no net change upon membrane interaction, indicating that CHX aggregation was not induced by their interaction with lipids. Some CHX-CHX interactions between the BGU and CPL regions were observed, but these did not persist for longer than a few nanoseconds (see Supplementary Figure 2). The density of the membrane components as a function of distance from the membrane centre was compared at the start and end of the simulations, revealing no obvious change in any repeat (see Supplementary Figure 3). Thus, binding of CHX to the membranes studied here did not cause any significant displacement of the membrane components.

The average APL of each membrane was calculated. The SaCM and EcIM membranes only exhibited a marginal difference when CHX was added which is further elaborated upon in sections pertaining to these membranes (see Supplementary Figure 4). This showed an increase of 0.09 and 0.01 $Å^2$ when CHX was added to the SaCM and EcIM systems respectively; this very small difference is due to CHX intercalating with the lipid headgroups, increasing the APL. It should be noted that as CHX was not restrained in the equilibration steps to allow for mixing, binding had already occurred at t = 0 ns. The EcOM did not show any significant difference between systems with or without CHX.

Chlorhexidine in alcohol solutions: Action on phospholipid membranes

To determine the effect of chaotropic sanitisers on phospholipid membranes alcohol and CHX were applied to the SaCM and EcIM. Given the intrinsic antibacterial activity of alcohol,[30–32] it is of interest to determine the additional impact of CHX. We therefore performed 200 ns comparative simulations of the two phospholipid bacterial membranes (SaCM, EcIM) in the presence of 20% w/v propanol (PROH) and isopropanol (ISOP) solutions with and without CHX, in triplicate. This concentration of alcohol was used because test systems using higher percentage solutions led to rapid membrane deformation, resulting in dramatic fluctuations in the semi-isotropically coupled unitcell and, consequently, simulation instability.

Simulated phospholipid membranes were surrounded by 0.5% w/v CHX in 0.15 M KCl with either 20% PROH or ISOP in bulk water on either side of the membrane. Visual inspection revealed rapid lipid dispersal in the SaCM (t = 45 and 50 ns for PROH and ISOP, respectively), becoming even more obviously deformed throughout the 200 ns of production simulation. This deformation was significantly faster in the EcIM system (t = 10 and 30 ns for PROH and ISOP, respectively). The timeframe for lipid dispersal was extrapolated from the rate of change of the width of each simulation box (see Supplementary Figure 5). Over the course of simulations, the lipids in these systems reoriented in a manner that disrupted the canonical bilayer structure of the membrane. Figure 3(a) shows that there is a significantly faster initial increase in APL for the EcIM when alcohol is applied, especially for PROH. This is due to the presence of hydrogen bonding between PG and LPG in the SaCM; these hydrogen bonds hold the headgroups together and provide an initial resistance to the dispersion caused by alcohol. However, this value plateaus at a lower value in the EcIM systems than in the SaCM ones, owing to a higher membrane charge in the SaCM (−0.3 e per lipid) compared to the EcIM (−0.15 e per lipid). Thus, the EcIM was impacted less by the alcohol/alcohol + CHX compared to the SaCM. This was evident from a gradual increase in APL which plateaued at a value approximately 80% greater than the equilibrated membrane for the SaCM systems and approximately 60% and 70% greater for the EcIM

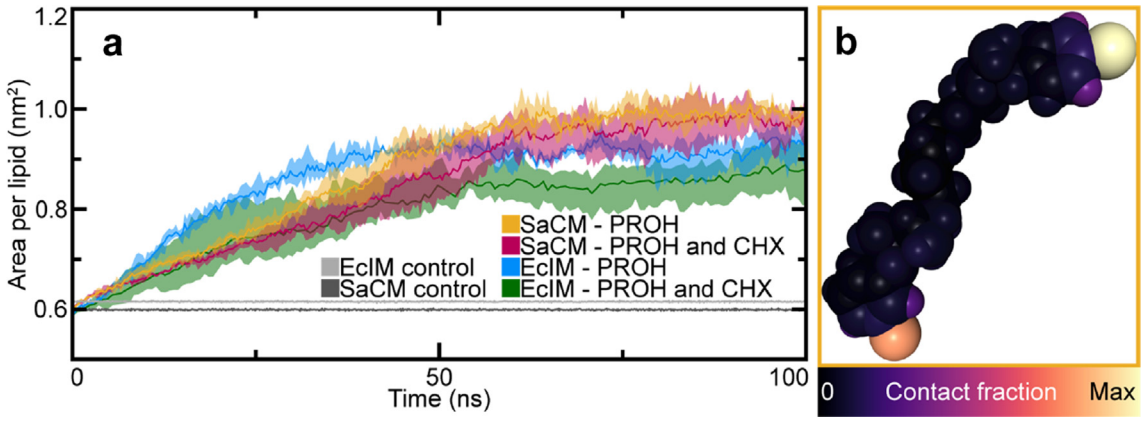

Figure 3. Analysis of the SaCM and EcIM when exposed to 20% w/v PROH solutions with and without CHX. (a) APL measurements of the SaCM and EcIM over the first 100 ns of production when exposed to PROH solutions with and without CHX, showing the average value after performing the experiment in triplicate as a full line and error between the repeats as a shaded region. APL measurements of the membranes in 0.15 KCl are shown in grey. (b) The structure of CHX heat mapped by the frequency of each atom contacting atoms in the headgroup of POPE over the final 20 ns of production.

systems both with and without CHX, respectively. The significantly lower final APL in the EcIM system which also contains CHX is due to interactions between the CHX terminal chlorines and NH_3+ functional groups in the headgroup of POPE which composes 90% of the bilayer. These interactions bind together lipid headgroups like a molecular staple. This results in a high proportion of contacts to chlorine within the CPL region of CHX while the rest of CHX experiences almost no interaction with the headgroups (Figure 3(b)). Analysis of the frequency of contacts of CHX with different lipids in the membrane was also performed (see Supplementary Figure 6). This showed far more frequent interaction with DPG in both PL membranes due to the size of the lipid, its greater anionic charge favoring binding to cationic CHX and the fact it contains more interfacial space for partitioning. Alcohol molecules became distributed further into the lipid core regions of the now very distorted bilayers, allowing the CPL regions of CHX to bind beneath the membrane surface at the headgroup-tail interfaces, as illustrated in Figure 2(b). This binding occurred regardless but was more rapid and significant when alcohol was present. The membrane deformation was characterized quantitatively by plotting the membrane density along the z-axis (parallel to the membrane normal, see Figure 4). System density plots also showed that alcohol distributed within the membrane by adopting energetically favourable positions at the headgroup/tail interface where it could minimise unfavourable interactions (Figure 4(b) and (d)); this positioning was seen in both PL systems. This positioning of PROH allowed the alcohol functional group to remain in the phosphate/ester region where it maintained polar interactions, while its hydrocarbon tail was able to form lipophilic interactions with the lipid tails regions, minimising interactions with water. To illustrate this, the lipids in the SaCM and EcIM model were mapped by their contacts with PROH and water. This clearly shows that alcohol accumulated significantly more around the headgroup/tail interface, where we propose it to take energetically stable conformations (Figure 5(a)). The absence of water interactions with the tails aligns with the observation that although significantly deformed, neither membrane allowed for pore formation. This observation is important as it shows that during early stages of deformation significant amounts of water did not enter the membrane. Snapshots of the hydrogen bonding occurring during simulations can be seen in Supplementary Figure 7. A similar effect was observed for systems containing ISOP, although the change in membrane deformation and APL was less dramatic since the branching in the secondary alcohol did not align as effectively with the lipid tails (see Supplementary Figure 8 and 9). This means the aliphatic chains cannot intercalate as effectively with the membrane tails, reducing the effect on the bilayer. In Figure 5(b) the location of PROH partitioning in the membranes was determined by plotting the time which 100 PROH molecules in the SaCM and EcIM system spend in contact with defined regions of the bilayer. A depiction of the defined regions is also given in Figure 5(c). The increased average residency time of PROH with the headgroups in the SaCM system is due to interactions with the large charged headgroup of LPG. The relatively well-defined residency time suggests that this is a strong interaction where PROH molecules occasionally get stuck. These results agree with

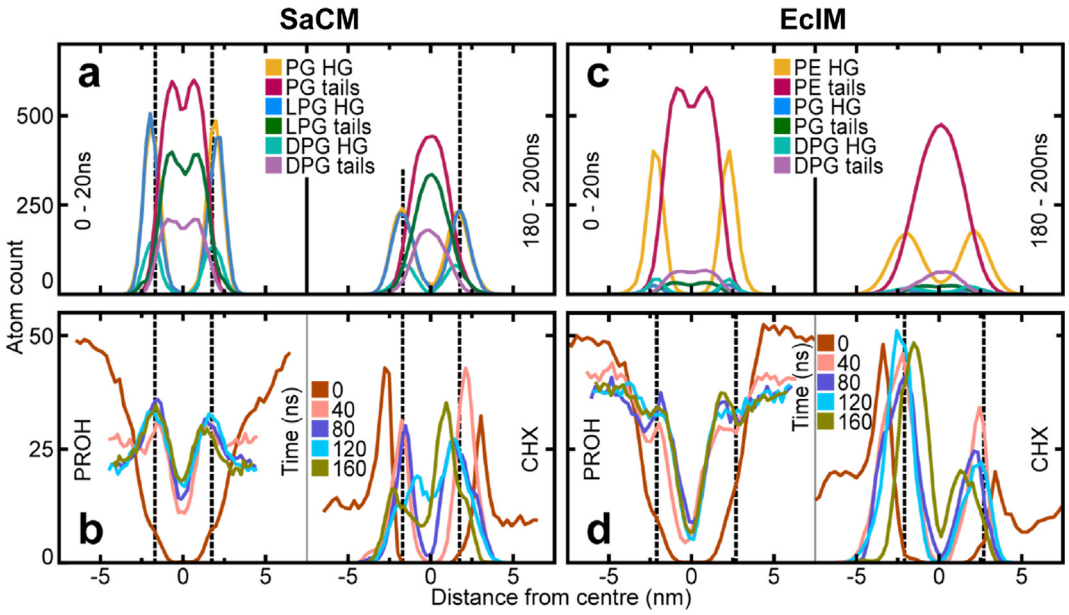

Figure 4. Measurements of the densities of membrane and sanitizer components along the z-axis of the simulation box in system exposed to both 20% w/v PROH and 0.5 w/v CHX together. (a) Densities of membrane components of the SaCM system exposed to PROH and CHX, averaged over the first and last 20 ns of production. (b) Densities of PROH and CHX in the SaCM system over time. (c) Densities of membrane components of the EcIM system exposed to PROH and CHX, averaged over the first and last 20 ns of production. (d) Densities of PROH and CHX in the EcIM system over time.

similar computational work performed by Ghorbani et al.[17] which found ethanol to accumulate at the headgroup/tail interface.

Analysis of system densities showed that CHX aggregated around the bilayer headgroups (Figure 4) where it interacted *via* the same c-shape interactions observed in the absence of alcohol. This mode of binding is especially favourable as its polar termini can form interactions with the phosphate/ester region of the lipids at the headgroup-tail interface. Although the 'wedge' conformation proposed by Komljenović et al.[18] was observed on occasion, it was far less common than the c-shape conformation. The results presented here for PL membranes are strongly supported by the findings of Rzycki et al.[33] who also observed CHX molecules may bind individually rather than in clusters, and those which did bind as an aggregate would rapidly disperse. Evidence of this dispersal is shown in Supplementary Figure 10. Similarly, they also found CHX to bind preferentially in the c-shape conformation and that the effect of CHX was minimal. Notably, density measurements of the system showed less aggregation of CHX on the membrane surface of the EcIM relative to the SaCM, again, presumably due to the lower membrane charge and the fact CHX is oppositely charged. Over the course of the 200 ns production run CHX molecules became bound by both of their BGU/CPL moieties which then became embedded within the headgroup-tail interface of the membrane (see Supplementary Figure 11. Interestingly, CHX 'bridging' was observed in the SaCM system; i.e. PROH caused significant deformation and thinning of the membrane such that CHX molecules bound to separate leaflets were able to contact each other across the bilayer, interacting *via* their BGU/CPL regions. However, there appeared to be no additional deformation compared to the alcohol systems which did not contain CHX. This phenomenon was not observed in the EcIM systems. This is reminiscent of the 'handshake' binding mode proposed by Komljenović et al.[18] Their findings suggest that CHX could operate *via* a similar mechanism to alcohol, by penetrating the membrane and aggregating in the membrane centre. However, this was not seen in simulations of CHX without alcohol. The SASA of CHX in these systems was tracked to determine whether CHX molecules had any tendency to cluster, but no indication of this was seen other than a dip for the SaCM system corresponding to a binding cluster of 4 CHX molecules which dissipated within 30 ns of forming on the bilayer surface (see Supplementary Figure 10). To ensure clustering was not significant, the average CHX separation was measured for systems both with and without alcohol, indicating it was not significant (see Supplementary Figure 12). This suggested the absence of clusters was due to CHX forming interactions with the membrane in preference to those it would form with itself. Contacts to CHX from the headgroups, interface and tails were also mapped. The CPL and to an extent BGU regions show most contacts with the

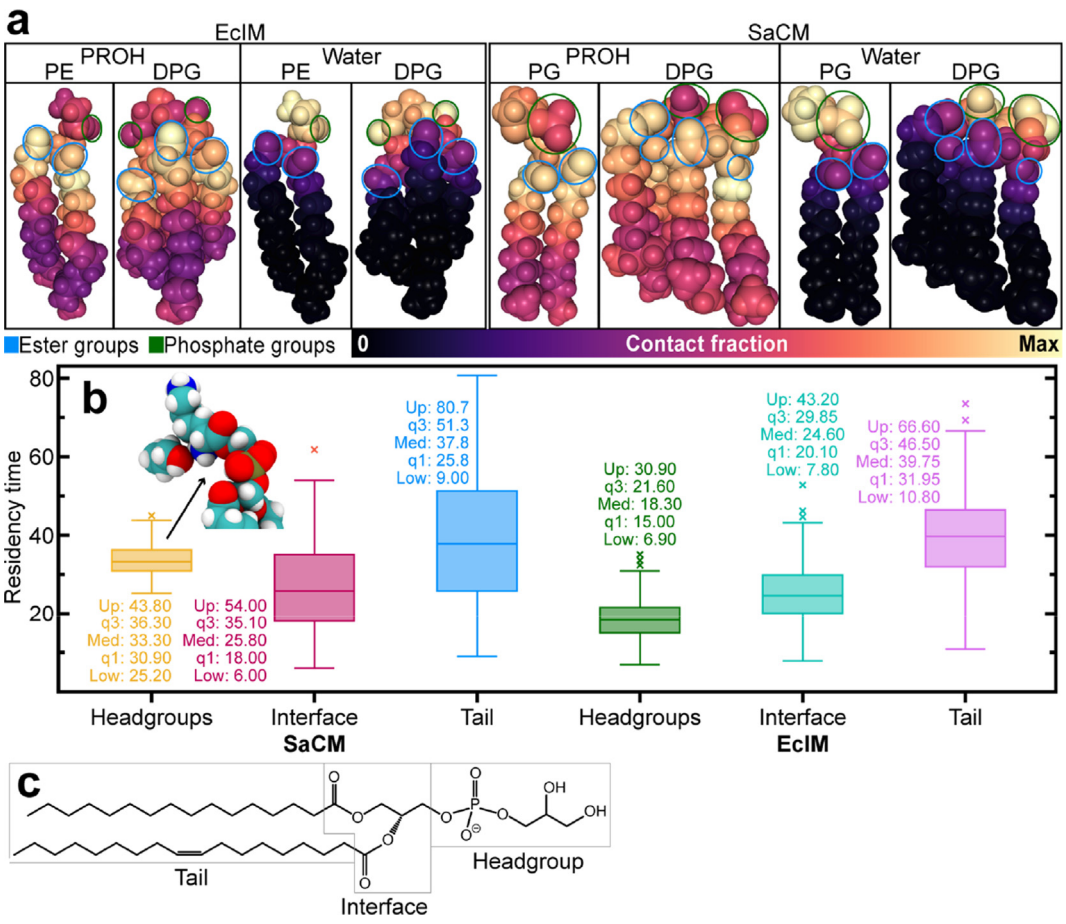

Figure 5. Analysis of the SaCM and EcIM when exposed to 20% w/v PROH and 0.5% w/v CHX in 0.15 M KCl. (a) Contact mapping of PE and DPG in the EcIM system and PG and DPG in the SaCM system , mapped for contacts with PROH and water separately. Contacts were taken from between 180 and 200 ns and mapped linearly from (black) the least to (yellow) the most contacts seen by any atom in the lipid, showing ester groups circled in blue and phosphate groups circled in green. (b) A box plot of the residency times of 100 PROH molecules in each repeat of the SaCM and EcIM systems over 200 ns of production to defined regions in the lipid bilayer and a representation of a significant PROH interaction with LPG headgroups in the SaCM. (c) A definition of the tails region (bellow the esters), the interface (between the esters and the phosphate group) and the headgroup (above the phosphate) using PE as an example.

lipid tails as they are embedded within the membrane, while the interface sees most of CHX. The only atom in CHX to significantly contact the headgroups was chlorine, due to a phenomenon where multiple NH_3+ groups would coorinate to the halide due to its large size and electronegativity. This is likely instrumental in the initial phases of CHX-membrane interaction, and the reason why CHX remains bound so tightly throughout production. This interaction is likely responsible for the significant reduction in lipid dispersal when CHX was added to the EcIM system without water.

Electroporation-driven insertion of CHX and effect of gluconate: MD study of the action on the EcIM

To eliminate the possibility that membrane permeation of CHX into the EcIM was not observed due to insufficient simulation sampling, we initiated simulations with CHX already placed in the core of the membrane. An external, constant electric field (0.125 V nm^{-1}) was applied across the EcIM to create a large water-filled pore. This method was adapted from a technique applied by Piggot et al.[34] to induce pore formation. This was performed so that a CHX molecule could be manually placed within this pore and the electric field then turned off to determine whether CHX would remain in the membrane core as the pore closed. Over the course of a 200 ns production run, CHX shifted from the membrane core to the same location as observed in the equilibrium simulations of CHX presented above (see Supplementary Figure 13). This behaviour was observed across three independent simulations of this system, providing conclusive support that the headgroup-lipid interface is the preferred location for CHX.

CHX is usually combined with gluconate (GLUC) in sanitising agents for increased solubility. To eliminate the possibility that GLUC is required to observe deep membrane penetration of CHX, we performed simulations including both molecules. 20 GLUC molecules were thus added to the bulk water (0.5% w/v) phase surrounding the EcIM (see Supplementary Figure 14). Following 100 ns of production simulations across three repeats, GLUC was not observed to penetrate the membrane and only briefly interacted with the surface (<1 ns events). Additional simulations in which 10 CHX molecules were added to the same system revealed the same CHX membrane binding mode as observed in simulations without GLUC. GLUC molecules were observed to regularly bind to the CPL regions of CHX, but this did not change the binding mode. (see Supplementary Figure 15).

Chlorhexidine in alcohol solutions: Action on the E. coli outer membrane (Ra-LPS)

The action of the chlorhexidine/alcohol solutions on the EcOM was next studied in the same way as for the PL membranes. The EcOM was extremely resistant to the deformation observed to be caused by alcohol in simulations of the PL membranes, despite the alcohol distributing within the membrane in the same way as for PL bilayers.[33] This is likely due to the strong interactions between LPS molecules and its stabilising 'cross-linking' calcium counter ions. Over the course of the first 60 ns (200 ns simulations in triplicate) there was no discernible change in the membrane structure in any of the EcOM simulations. By this time both PL membranes (SaCM and EcIM) had shown significant deformation due to alcohol partitioning in the headgroup/tail interface. Due to the retained integrity of the EcOM there was little change when analyzing the bilayer density, other than a small shoulder of budding lipids (see Supplementary Figure 16). By 80 ns the PL leaflet of the EcOM began to form a small bundle of approximately 50 lipids which started to separate from the membrane (Figure 6(a)). The budding phenomenon was observed in two of the three repeats with PROH but none of the repeats performed in ISOP (see Supplementary Figure 17). PROH distributes into the lipid headgroup/tail interface of both leaflets, whereas ISOP did not distribute into the interface as effectively because of its branched structure. Partitioning of alcohol into the membrane disperses the bilayer components due to crowding. This was alleviated in the PL membranes by lateral dispersal, however due to the calcium cross-linked LPS molecules lateral movement was prevented here. This resulted in the PL leaflet budding into the periplasmic space to relieve the crowding, forming a shell of polar lipid headgroups sheltering their

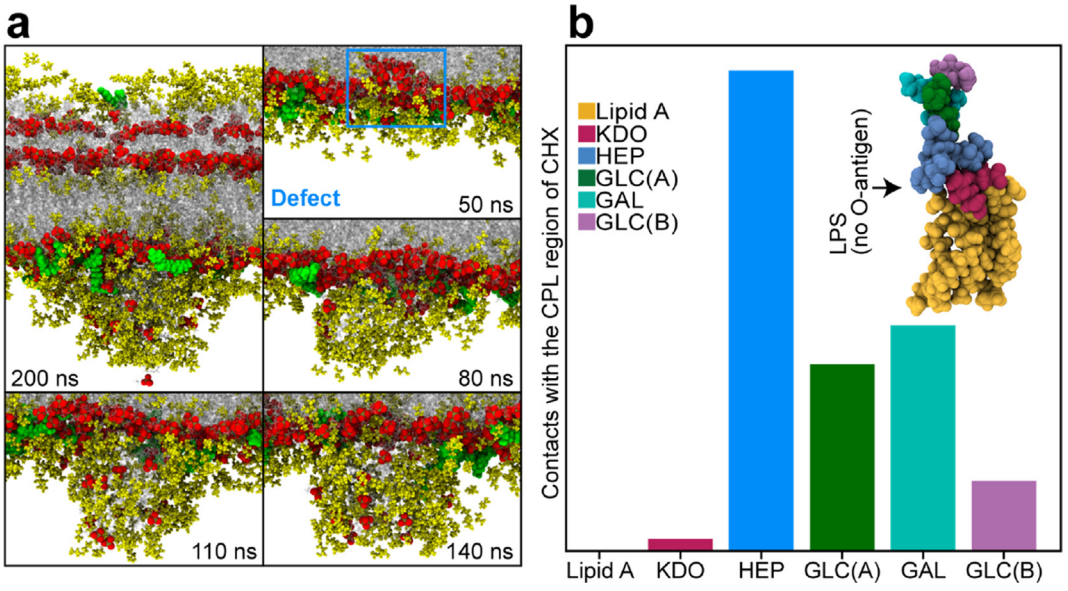

Figure 6. (a) Snapshots of the EcOM exposed to 0.5% w/v CHX in 20% PROH at 200 ns with further snapshots of the PL leaflet at 50, 80, 110 and 140 ns, showing phosphate oxygen as spheres in red, phosphate phosphorous in gold, CHX in green, PROH within 10 Å of the membrane in yellow and lipids as translucent. (b) The proportion of contacts between the CPL region of CHX and sugars in LPS tracked over the full 200 ns of production by checking at each time step how many contacts there were within 2.5 Å of the CPL region and adding them to the total count per sugar, showing lipid A in yellow, ketodeoxyoctonic acid (Kdo) in red, Heptose (HEP) in blue, Glucose (GLC) A in green, Galactose (GAL) in cyan and Glucose B in pink. Glucose are labelled A and B as they are in two different positions.

hydrophobic tails. As a small amount of both alcohols was able to pass through the LPS leaflet regularly, this showed that deformation is possible with alcohol entering from only the extra-cellular leaflet, as expected physiologically. Given enough time to penetrate the membrane solely from the LPS leaflet side, build up of lateral pressure may result in budding to such a degree that it entirely deforms the EcOM. As commercial sanitizers contain more alcohol (~70% w/v) this may be expected to occur at an even faster rate than observed here.

Visual analysis of the production runs showed that only one CHX molecule ever became bound to the LPS leaflet in any of our simulations, and in three out of six simulations with alcohol and CHX present, none became bound to the LPS leaflet (2 of 3 PROH repeats and 1 of 3 ISOPR repeats). The lack of binding to the LPS leaflet was due to the significantly fewer favourable interactions between the HEX region of CHX and LPS sugars. Generally CHX became bound to the heptose moeity in the LPS sugar region and did not translocate any further (Figure 6(b)). A summary of the interaction of the LPS leaflet with CHX is shown in Supplementary Figures 18 and 19.

Chlorhexidine and propanol: ^{31}P NMR study of their action upon the structure of the E. coli inner membrane

The action of sanitizer components on the structure of the EcIM model was next assessed experimentally using ^{31}P solid-state NMR. This method produces a lineshape characteristic of the dynamics and phase of a lipid bilayer. Spectra were acquired of multilamellar vesicles composed of PE/PG/CL (90/5/5 mol%) exposed to PROH, GLUC and chlorhexidine gluconate (CHG) to assess their influence on the bilayer structure (Figure 7). Chlorhexidine gluconate is chlorhexidine with the gluconate counter ion; this salt form of CHX is used in experiments as it greatly increases the solubility of CHX with no effect on its ability to act as a sanitizing agent.

As expected in the absence of any reagents, the ^{31}P spectrum of the model EcIM exhibited an axially symmetrical lineshape, with a chemical shielding anisotropy of 43 ppm, consistent with the lipids existing in the liquid crystalline phase. Increasing the concentration of PROH in the sample resulted in significant perturbations of the bilayer structure (Figure 7(b-f)). Up to 40% the lipids retained their bilayer character, with a slight reduction in the chemical shielding anisotropy indicative of increased headgroup mobility. This was consistent with the partitioning of the PROH at the top of the lipid chains which would result in a lower lateral pressure in the headgroup region. Between 40% and 60% w/v PROH most of the bilayer structures were solubilised with the spectra dominated by an isotropic signal at −0.1 ppm, with only a minor bilayer-like component still present at 60% PROH.

To assess the influence of CHG on the bilayer structure the ^{31}P lineshape was measured at concentrations up to 4% w/v (Figure 7(h-k)) as this is the highest concentration commonly used in commercial sanitizers. Increasing concentrations of CHG had limited influence on the ^{31}P lineshape, with all spectra showing a characteristic axially symmetric lineshape indicative of a bilayer like phase. Notably there was a slight increase in the chemical shielding anisotropy as the concentration increased, suggesting that the CHG may limit headgroup mobility. This was also reflected in subtle changes in the lineshape. Increases in the intensity on the downfield edge and overall broadening of the spectral features were similar to those observed in the gel phase and which are typically attributed to a reduction in T_2 of the phosphates in the headgroup. This suggests that the bilayer became more rigid and less elastic, likely due to CHG binding holding lipid headgroups together, as observed *via* MD simulation.[35–39]

Similar observations were seen upon the addition of GLUC with the spectra (Figure 7(g)) exhibiting similar broadening due to a reduction in T_2, although no changes in the relative intensity across the lineshape were observed, thereby suggesting that GLUC had minimal influence on bilayer elasticity. These effects appeared to be mediated by CHX, as the corresponding spectrum of 4% GLUC exhibits a classical axially symmetric lineshape expected from multi lamellar vesicles (MLVs).

Chlorhexidine and propanol: An ^{1}H MAS NMR study of their location within the E. coli inner membrane

To investigate the location of the CHG within the model EcIM, ^{1}H-MAS and 2D ^{1}H/^{1}H MAS-NOESY experiments were recorded. Due to the high mobility within the lipid bilayer the ^{1}H spectra were well resolved, as previously reported.[14,40] The 1H spectrum of the model EcIM was dominated by resonances from POPE, the major lipid species in this system. The resonances from the lipids were assigned based on published assignments of POPC and POPE (Figure 8).[14] To assist in the assignment of the components present in sanitizer, the individual PROH, GLUC and CHG components were added to the EcIM independently. Addition of 20% PROH gave rise to three major resonances at 3.61, 1.61 and 0.96 ppm whilst the addition of GLUC gave rise to a family of resonances superimposed on lipid signals assigned to G1, G3, α and β. Assignments were made based on published values and are shown in Figure 8.[30] The addition of CHG resulted in the appearance of a further 6 resonances which were assigned to CHX, with those in the aromatic structure clearly resolved (Figure 8

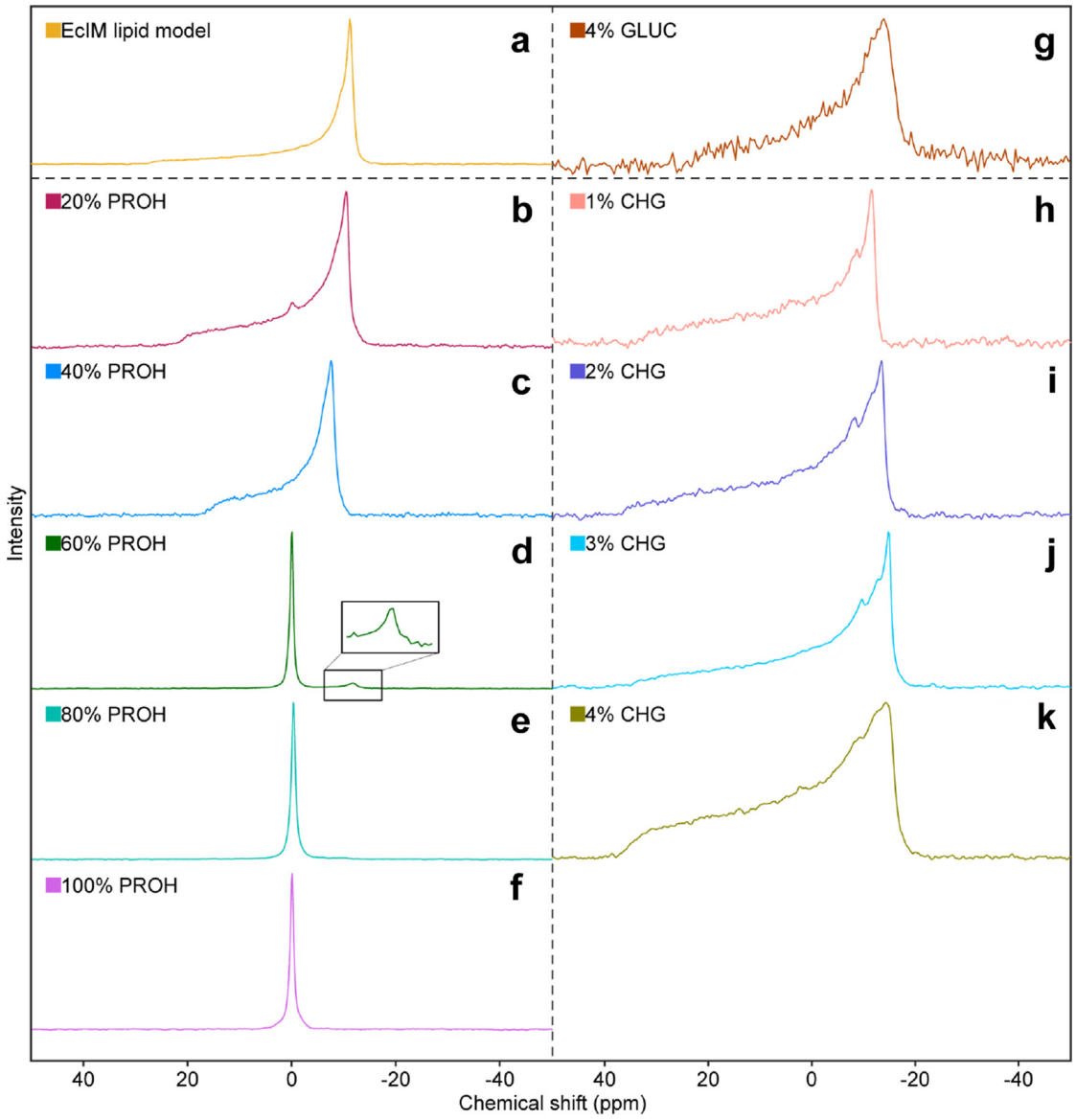

Figure 7. Static ^{31}P NMR spectra of the EcIM model (A) alone, with PROH at (B-F) 20% w/v intervals, with (G) 4% w/v GLUC and with CHX (H-K) up to 4% at 1% w/v intervals. The area marked by an asterisk is the emerging environment which was witnessed in the CHX experiments.

(d) - proton assignments 1 and 2), whilst those from the BGU/HEX appearing amongst the resonances arose from the lipids in the sample (Figure 8(d) - proton assignments 3,4 and 5). Closer inspection showed that resonances arising from the C2, C3 and G2 sites within the lipid were shifted upon the addition of CHG. It is plausible that the presence of the CPL groups at the headgroup-tail boundary may have generated ring-current effects resulting in the observed perturbations, in a manner similar to that reported for ibuprofen by Kremkow et al.[41] Close inspection of the CPL region of the spectrum (Figure 8(f)) revealed that CHG exhibited three resonances in the aromatic region, which was unexpected given the presence of only two resonances for the aromatic protons in the CPL groups in CHX and the expected magnetic equivalence of the protons on either side of the aromatic ring. We suggest that the additional resonance arose due to a stable complex of CHX and GLUC, formed by interaction of the CPL region of CHX with the carboxylic acid group of GLUC (Figure 8(g)). This would break the magnetic equivalence and perturb the C2 shift in a manner similar to that observed. This was supported by the complexes seen in MD simulations of CHX with GLUC (Figure 8(e)).

Chlorhexidine: A ^{1}H NOESY MAS NMR study of their location within the E. coli inner membrane

To establish a more detailed idea of the average location of the CHX within the membrane, 2D 1H/1H NOESY MAS NMR spectra were recorded.

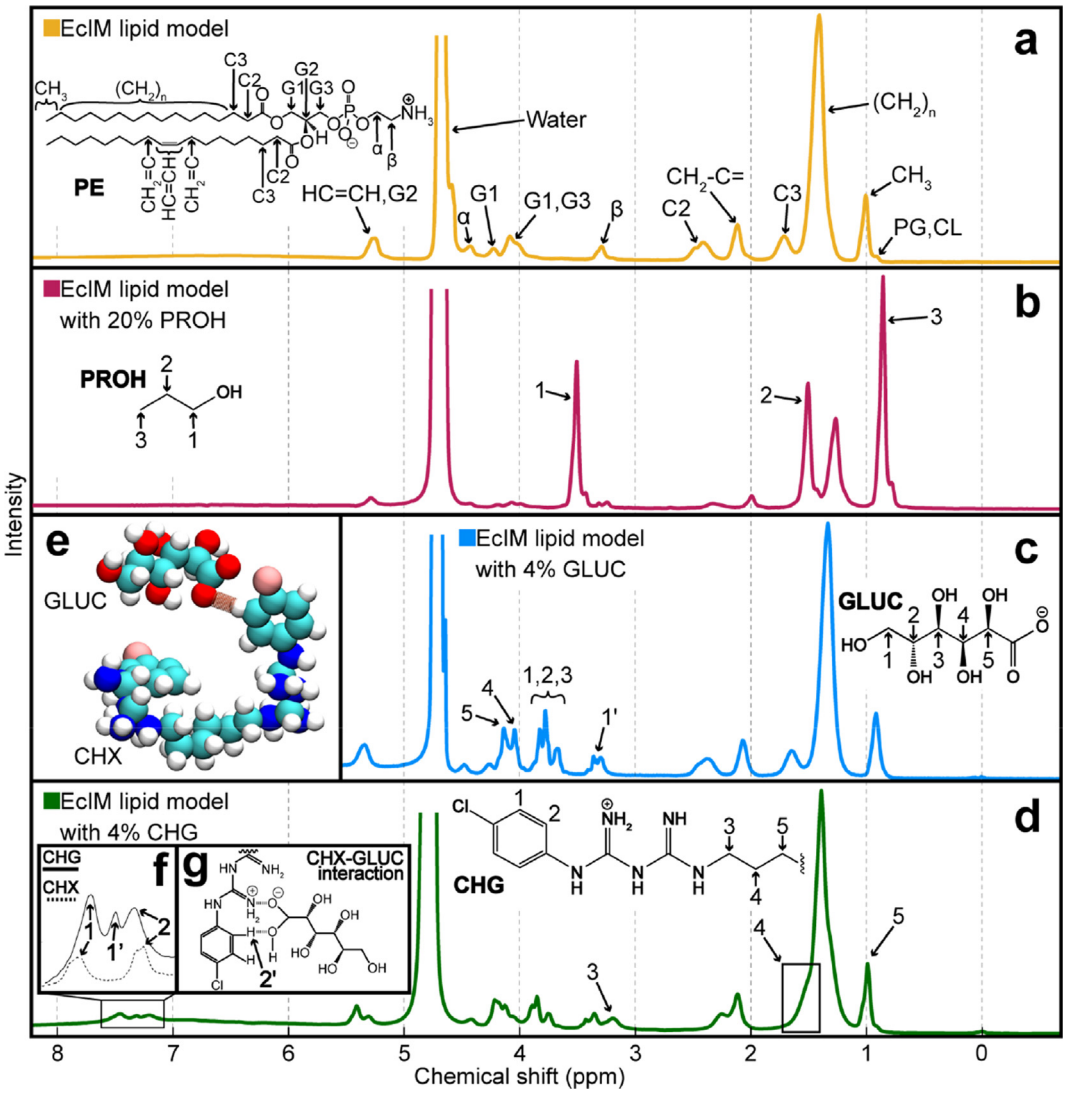

Figure 8. Assignment of the ^{1}H NMR spectra of (A) the EcIM model alone in water, (B) with 20% w/v PROH, (C) with 4% w/v GLUC and (D) with 4% w/v CHG. (E) A visual representation of a common interaction between CHX and GLUC in an MD simulation of 10 CHX and 20 neutralising GLUC. Atoms are shown as spheres, hydrogen in white, carbon in cyan, nitrogen in blue, chlorine in pink, oxygen in red and hydrogen bonding in brown. (F) Resonances arising from CHX and CHG. (G) A mechanistic depiction of the interaction between CHX and GLUC which is theorised to account for the additional resonance.

The dynamics present in the membrane give rise to the well resolved 1H spectra, at moderate MAS frequencies, allowing the analysis of NOE based magnetization exchange. The intensity of the cross-peaks in the 2D 1H/1H NOESY MAS NMR reflect the residency time and proximity of protons with respect to one another.[42] As shown in previous research,[42–44] an analysis of the intermolecular cross-relaxation rates between resonances arising from the small molecule and the lipids can provide a valuable insight into the partitioning and location of small molecules within the lipid bilayer. CHG was applied to the membrane at a concentration of 4% w/v (Figure 9. Although the percentage volume was much larger, due to the size of CHG the molar ratios of PROH and CHG to lipids are similar (1:4.67 and 4.12 respectively). There were significant intramolecular cross-peaks between the resonances arising from the CHG, most clearly defined with sites in the CPL rings and less clearly between the HEX resonances which were poorly resolved from lipid resonances. Inter-molecular cross-peaks were also apparent; these were most clearly observed between the CPL protons and the intense signal from the CH_2 moieties in the lipid chains. Lower intensity peaks were also apparent between the CPL protons and those from the protons at C2 and the glycerol backbone. This data again indicates

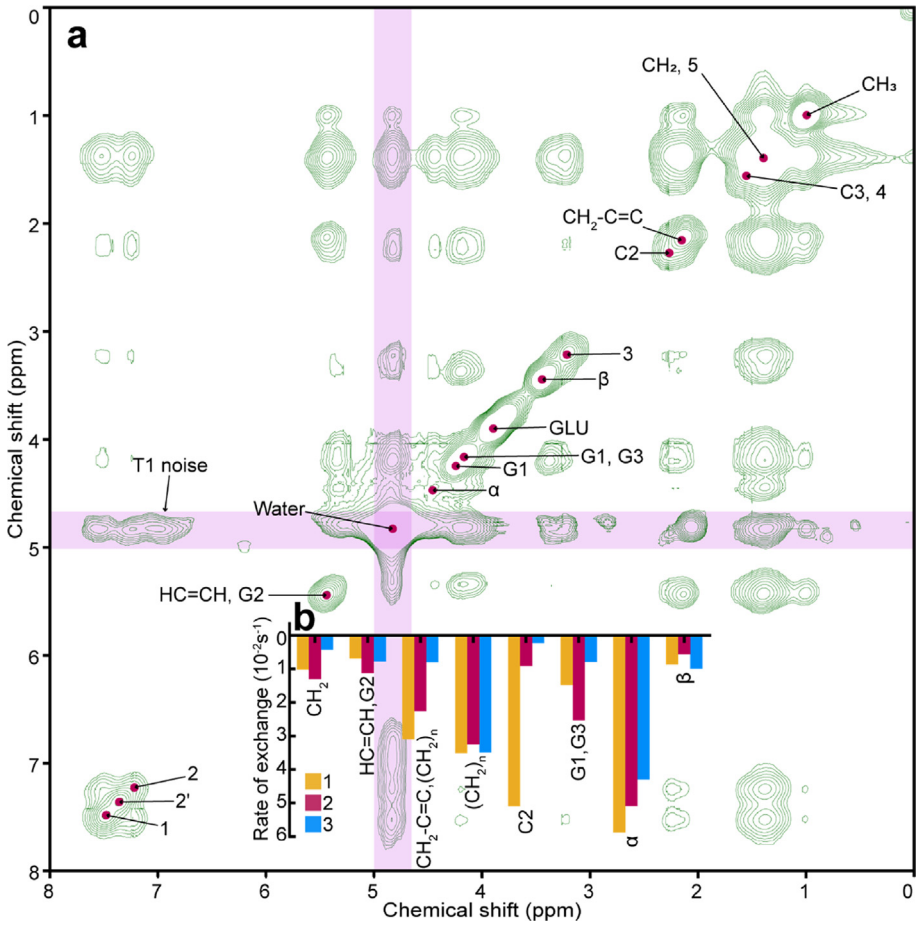

Figure 9. Assignment of 2D NOESY spectrum of the EcIM model membrane when exposed to CHG for calculation of magnetisation exchange rates between protons in the system. (a) The two-dimensional NOESY NMR spectrum of the EcIM model exposed to CHG at a concentration of 4% w/v with a 250 ms mixing time. Positive contours are shown in green and peaks are indicated by a mark in red. Areas which are distorted due to t_1 noise are highlighted in pink. (b) A bar chart of the magnetisation exchange rate of the protons 1, 2 and 3 with protons in lipids in the EcIM lipid bilayer model, ordered from left to right to represent groups ascending from the bilayer centre toward the top of the lipid headgroup.

that CHG has a preferred localisation at the level of the glycerol backbone in the lipid bilayer. Weak correlations were also seen between the C3 and the lipid resonances, indicating that the backbone of the CHG was lying in the plane of the membrane, in agreement with the MD simulations presented above. To ascertain the relative orientation of CHG within the EcIM, a quantitative analysis of the cross-relaxation rates was performed (Figure 9(b)). Interestingly, the cross-relaxation rates suggest that resonances 1 and 2 interacted favourably with sites spanning the region from the unsaturated site within the lipid chains (HC = CH), up to the region of the lipid backbone. In contrast, cross-relaxation of resonance 3 was dominated by exchange to the α proton of the PE headgroup, suggesting that the BGU/HEX groups of CHG prefer to localise within the region of the lipid headgroups, in keeping with the membrane bound position observed during simulation.

Conclusions

The simulation and NMR studies described here provide insights into the mode of action of the common sanitizing agent CHX on *S. aureus* and *E. coli* membranes. We find that in the aqueous solution (no alcohol), CHX binds and inserts into the PL membranes (SaCM and EcIM) and maintains a position at the headgroup/tail interface of the latter, while moving slightly deeper into the former. Intriguingly, insertion of CHX does not induce disruption of the membranes during the timescales of the MD simulations. Nevertheless, CHX was found to reduce the MSD of lipids due to binding and holding together of headgroups, thereby acting as a 'molecular staple'. This result also supports a previously suggested mechanism.

No insertion of CHX into the LPS leaflet of the EcOM was observed in the MD simulations. This

is likely due to limitations in timescale exacerbated by the slow-moving nature of LPS. We note that similar lack of penetration of other cationic antimicrobial agents such as polymyxins has previously been reported from atomistic MD simulations.[45] Nevertheless, the comparative simulations show a greater kinetic barrier to entry into the outer membrane compared to the PL membranes.

Inclusion of alcohol, PROH or ISOP, had a dramatic impact on the PL membranes. Both alcohols were seen in multiple simulation replicas to cause significant deformation of both the EcIM and SaCM. Although alcohol-induced deformation of PL membranes is not a novel finding, contact tracking showed that deformation is the product of many transient residencies of alcohol in energetically beneficial positions within the bilayer. Large quantities of alcohol partitioning into this region resulted in lateral dispersion of lipids which caused significant deformation; at larger alcohol concentrations this leads to dissolution of the membrane. The same effect seen for PL membranes was not seen for the EcOM due to the lateral interactions between components of the LPS leaflet and calcium which are significantly stronger compared to either PL membranes. Restrictions imposed by the LPS leaflet meant that the bilayer could not disperse to alleviate steric crowding. This caused the PL leaflet to 'bud' into the solution as this was the only way to reduce the crowding created by alcohol partitioning.

Solid-state 1D proton NMR studies corroborate the findings of the simulations with specific peaks in the 1D NMR spectra which confirm the CPL groups in CHX bind to the membranes, as predicted computationally. This was then examined in greater detail by exploring the magnetisation exchange rates which were seen for specific protons in CHX. This showed that the binding of CPL in CHX was not only in the same position as observed in simulation, but also adopted the same orientation.

Static ^{31}P solid state NMR showed *via* perturbations in lineshape of the MLV that increases in the concentration of alcohol deformed and then dissolved the MLV, as expected. Increasing the concentration of CHX from 1-4% w/v did not lead to destruction of the MLV bilayer. Very minor changes in the line shape, contrarily, suggested an increase in the rigidity of the MLV bilayer. This finding was corroborated by the lower MSD of lipids in the simulated EcIM and SaCM systems when CHX was applied; decreased mobility implies greater membrane rigidity.

These data have successfully begun to elucidate key details regarding the modes of action of sanitizer components when applied to common bacterial membranes. By studying the differences between these systems, we can begin to further develop chemicals to improve their membrane destructive properties, particularly in light of growing antimicrobial resistance. In future studies we aim to include other membrane bound molecules such as proteins, against which sanitizers may also act. A coarse-grained approach with CHX would also allow us to overcome sampling limitations and what changes may be induced when observed over significantly longer timeframes. Broadening our approach to these systems will allow us to further assess what is currently limiting the sanitizers we currently rely upon and how bacteria may evolve to counter them.

Methodology

Simulation system setup and model parameters

Aqueous alcohol and CHX solutions were constructed at the desired concentration (20% and 0.5% w/v respectively) before performing equilibration and production. Membranes were surrounded by an aqueous KCl (0.15 M) solution before equilibration and separate production prior to simulation with alcohol or CHX. A series of tests of CHX behaviour at different KCl concentrations in solution were performed to select optimal salt conditions, as described in Supplementary Material. Alcohol solutions were applied to both faces of the membrane by removing water from the membrane system and adding the aqueous alcohol solution in the cleared space, without removing KCl. Chlorhexidine was parameterised *via* the CHARMM-GUI with standard parameters from the CHARMM General Force Field (CGenFF), yielding no significant penalties for any parameters. The overall ionization state of the molecule was chosen to be +2e, based on prior simulation studies which showed this gave best agreement with membrane partitioning data from neutron scattering and NMR experiments.[57–58]

Simulation protocols

Simulations were set up and performed using the GROMACS[46–48] molecular dynamics software package (version 2020.2) with the CHARMM36 force field.[49–50] Systems were maintained at a temperature of 310 K, using the Nosé-Hoover[51–52] thermostat with a time constant of 1 ps. The pressure of the system was maintained at 1 atm, with a time constant of 2 ps, using semi-isotropic pressure coupling with the Parrinello-Rahman[53–54] barostat. All van der Waals interactions were cut off at 1.2 nm and a smooth particle mesh Ewald[55] (PME) algorithm was used to treat electrostatic interactions with a real space cut off of 1.4 nm. Simulation parameters were chosen based on similar published studies of Piggot et al.[34] For equilibration, each system was subjected to 500 ps of NVT simulation, followed by 2 ns of NPT. Positional restraints (1000 kJ mol^{-1} nm^2) were placed on the membrane

headgroup atoms during NVT and NPT equilibration. Production simulations were then performed without any positional restraints. The results were analysed using GROMACS tools and in-house scripts. Visualisation was performed using the visual molecular dynamics (VMD)[56] software package. Electroporation of the membrane was performed with a 0.125 V nm^{-1} electric field applied along the membrane normal.

Calculating proportion of sugar interactions with the CPL region of CHX

The full 200 ns of production was parsed through a python script written in Jupyter Notebooks[59] which checked each timeframe for contacts within 2.5 Å of the CPL region *via* MDAnalysis[60] and then used this information to create a bar chart with Matplotlib.[61]

Experimental sample preparation

Lipid samples were prepared from a stock solution of PE, PG and DPG in a ratio of 90:5:5 respectively. Stocks were placed in ethanol at a lipid concentration 10 mg ml^{-1}. Samples of 5 mg lipid mixtures were left under high-vacuum to remove residual solvent. The lipids were rehydrated in 20 μL of D_2O (25% w/v) containing alcohol or chlorhexidine at the appropriate concentration. Samples containing 5 mg of lipid were freeze-thawed 5 times. Each cycle involved placing the sample in liquid nitrogen, thawing and mixing with a vortex mixer. These samples were then transferred to 3.2 mm rotors.

Solid-state NMR

Solid-state NMR spectra were recorded on a 600 MHz Agilent DD2 NMR spectrometer (Yarnton, UK), equipped with a 3.2 mm triple resonance MAS NMR probe. All spectra were acquired at 25 °C unless specified. Static ^{31}P spectra were recorded with a Hahn-echo pulse sequence[62] with a 3.5 ms excitation pulse, 70 kHz proton decoupling during acquisition and a 50 ms echo time. A 2.5 second recycle delay was employed to minimise sample heating. All ^{31}P spectra were externally referenced to H_3PO_4 (85%). Prior to Fourier transformation data was left shifted to the top of the echo, zero filled to 2048 points and 100 Hz linebroadening was applied.

All proton spectra were record with 12.5 kHz MAS, and a 2.75 ms pulse for excitation, and a 2.5 second recycle delay. All proton spectra were acquired with the probe with the X channel tuned to deuterium and connected to the spectrometers lock allowing the stabilization of the field which significantly reduced t_1 noise in 2D spectra. Proton spectra were referenced to the residual water peak at 4.65 ppm. 2D ^{1}H–^{1}H MAS-NOESY spectra were recorded using a standard exchange sequence[63] with States-TPPI in the indirect dimension.[64] Data was processed with in NMRpipe[65] or Matlab[66] using matNMR.[67]

Matrix based approach to NOESY magnetisation exchange rates

Using the two-dimensional NOESY spectra acquired, the rate of exchange of magnetisation for protons in the system were calculated *via* a full matrix approach based on the Solomon equations.[43] Peak volumes were integrated using the ccp NMR software.[68] The resulting volume matrices were then normalised and used to calculate the cross-relaxation rates according to Supplementary Equation 1 using custom written scripts in Matlab (Mathworks).

Funding

CW and EM are supported by the ARAP program via the University of Southampton and A*STAR Graduate Academy (A*GA). SK is funded by Engineering and Physical Sciences Research Council (Grant No EP/V030779 and EP/R029407). We gratefully acknowledge the provision of High-Performance Computing time on ARCHER and ARCHER2 via HECBioSim (Engineering and Physical Sciences Research Council grant number EP/R029407). PJB and JKM are grateful to BII (A*STAR) core funds.

The funders had no role in study design, data collection and analysis, decision to publish, or preparation of the manuscript.

CRediT authorship contribution statement

Callum Waller: Formal analysis, Investigation, Methodology, Validation, Visualization. **Jan K. Marzinek:** Formal analysis, Methodology, Validation. **Eilish McBurnie:** Formal analysis, Investigation, Methodology, Validation, Visualization. **Peter J. Bond:** Conceptualization, Formal analysis, Funding acquisition, Resources, Supervision. **Philip T.F. Williamson:** Conceptualization, Formal analysis, Funding acquisition, Investigation, Methodology, Project administration, Resources, Supervision, Validation. **Syma Khalid:** Conceptualization, Formal analysis, Funding acquisition, Investigation, Methodology, Project administration, Resources, Supervision, Validation.

DECLARATION OF COMPETING INTEREST

The authors declare that they have no known competing financial interests or personal relationships that could have appeared to influence the work reported in this paper.

Appendix A. Supplementary Data

Supplementary data to this article can be found online at https://doi.org/10.1016/j.jmb.2023.167953.

Received 18 September 2022;
Accepted 4 January 2023;

Keywords:
Bacteria;
NMR;
MD;
partitioning;
deformation

Abbreviations:
CHX, Chlorhexidine; CHG, Chlorhexidine Gluconate; CPL, Chlorophenyl; BGU, Biguanide; HEX, Hexane; APL, Area Per Lipid; SaCM, *S. aureus* cell membrane; EcIM, *E. coli* inner membrane; EcOM, *E. coli* outer membrane; LPS, Lipopolysaccharide; PE, Phosphoethanolamine; PG, Phosphoglycerol; DPG, Cardiolipin; LPG, Lysyl-Phosphatidylglycerol; SASA, Solvent Accessible Surface Area; PROH, Propanol; ISOP, Isopropanol; GLUC, Gluconate; VMD, Visual Molecular Dynamics; NOESY, Nuclear Overhauser Effect Spectroscopy

References

1. Perry, J., Waglechner, N., Wright, G., (2016). The prehistory of antibiotic resistance. *Cold Spring Harb. Perspect. Med.* **6** https://doi.org/10.1101/cshperspect.a025197.
2. Morehead, M., Scarbrough, C., (2018). Emergence of global antibiotic resistance. *Primary Care: Clin. Off. Practice.* **45**, 467–484.
3. Blaney, D.D., Daly, E.R., Kirkland, K.B., Tongren, J.E., Kelso, P.T., Talbot, E.A., (2011). Use of alcohol-based hand sanitizers as a risk factor for norovirus outbreaks in long-term care facilities in northern New England. *Am. J. Infect. Control* **39**, 296–301. https://doi.org/10.1016/j.ajic.2010.10.010.
4. Fendler, E.J., Ali, Y., Hammond, B.S., Lyons, M.K., Kelley, M.B., Vowell, N.A., (2002). The impact of alcohol hand sanitizer use on infection rates in an extended care facility. *Am. J. Infect. Control* **30**, 226–233. https://doi.org/10.1067/mic.2002.120129.
5. Hilburn, J., Hammond, B.S., Fendler, E.J., Groziak, P.A., (2003). Use of alcohol hand sanitizer as an infection control strategy in an acute care facility. *Am. J. Infect. Control* **31**, 109–116. https://doi.org/10.1067/mic.2003.15.
6. Lim, K.S., Kam, P.C.A., (2008). Chlorhexidine - Pharmacology and clinical applications. *Anaesth Intensive Care* **36**, 502–512. https://doi.org/10.1177/0310057x0803600404.
7. Gomes, B.P.F.A., Vianna, M.E., Zaia, A.A., Almeida, J.F. A., Souza-Filho, F.J., Ferraz, C.C.R., (2013). Chlorhexidine in endodontics. *Braz. Dent. J.* **24**, 89–102. https://doi.org/10.1590/0103-6440201302188.
8. Russell, A.D., Day, M.J., (1993). Antibacterial activity of chlorhexidine. *J. Hosp. Infect.* **25**, 229–238.
9. Adams, D., Quayum, M., Worthington, T., Lambert, P., Elliott, T., (2005). Evaluation of a 2% chlorhexidine gluconate in 70% isopropyl alcohol skin disinfectant. *J. Hosp. Infect.* **61**, 287–290. https://doi.org/10.1016/j.jhin.2005.05.015.
10. Ingram, L.O., (1981). Mechanism of lysis of Escherichia coli by ethanol and other chaotropic agents. *J. Bacteriol.* **146**, 331–336. https://doi.org/10.1128/jb.146.1.331-336.1981.
11. Mcdonnell, G., Russell, A.D., Operations, L., Louis, S., (1999). Antiseptics and disinfectants: activity, action, and resistance. *Clin. Microbiol. Rev.*.
12. Tóth, M.E., Vígh, L., Sántha, M., (2014). Alcohol stress, membranes, and chaperones. *Cell Stress Chaperones* **19**, 299–309. https://doi.org/10.1007/s12192-013-0472-5.
13. Foddai, A.C.G., Grant, I.R., Dean, M., (2016). Efficacy of instant hand sanitizers against foodborne pathogens compared with hand washing with soap and water in food preparation settings: A systematic review. *J. Food Prot.* **79**, 1040–1054. https://doi.org/10.4315/0362-028X.JFP-15-492.
14. Feller, S.E., Brown, C.A., Nizza, D.T., Gawrisch, K., (2002). Nuclear Overhauser enhancement spectroscopy cross-relaxation rates and ethanol distribution across membranes. *Biophys. J.* **82**, 1396–1404. https://doi.org/10.1016/S0006-3495(02)75494-5.
15. Overhauser, A.W., (1953). Polarization of nuclei in metals. *Phys. Rev.* **92**, 411–415. https://doi.org/10.1103/PhysRev.92.411.
16. Patra, M., Salonen, E., Terama, E., Vattulainen, I., Faller, R., Lee, B.W., Holopainen, J., Karttunen, M., (2006). Under the influence of alcohol: The effect of ethanol and methanol on lipid bilayers. *Biophys. J.* **90**, 1121–1135. https://doi.org/10.1529/biophysj.105.062364.
17. Ghorbani, M., Wang, E., Krämer, A., Klauda, J.B., (2020). Molecular dynamics simulations of ethanol permeation through single and double-lipid bilayers. *J. Chem. Phys.* **153** https://doi.org/10.1063/5.0013430.
18. Komljenović, I., Marquardt, D., Harroun, T.A., Sternin, E., (2010). Location of chlorhexidine in DMPC model membranes: A neutron diffraction study. *Chem. Phys. Lipids* **163**, 480–487. https://doi.org/10.1016/j.chemphyslip.2010.03.007.
19. van Oosten, B., Marquardt, D., Harroun, T.A., (2017). Testing high concentrations of membrane active antibiotic chlorhexidine via computational titration and calorimetry. *J. Phys. Chem. B* **121**, 4657–4668. https://doi.org/10.1021/acs.jpcb.6b12510.
20. Müller, G., Langer, J., Siebert, J., Kramer, A., (2014). Residual antimicrobial effect of chlorhexidine digluconate and octenidine dihydrochloride on reconstructed human epidermis. *Skin Pharmacol. Physiol.* **27**
21. Karpanen, T.J., Worthington, T., Conway, B.R., Hilton, A. C., Elliott, T.S.J., Lambert, P.A., (2008). Penetration of chlorhexidine into human skin. *Antimicrob. Agents Chemother.* **52**, 3633–3636. https://doi.org/10.1128/AAC.00637-08.
22. Lugtenberg, E.J.J., Peters, R., (1976). Distribution of lipids in cytoplasmic and outer membranes of Escherichia coli K12. *BBA* **441**, 38–47.
23. Sohlenkamp, C., Geiger, O., (2015). Bacterial membrane lipids: Diversity in structures and pathways. *FEMS*

Microbiol. Rev. **40**, 133–159. https://doi.org/10.1093/femsre/fuv008.
24. Rowlett, V.W., Mallampalli, V.K.P.S., Karlstaedt, A., Dowhan, W., Taegtmeyer, H., Margolin, W., Vitrac, H., (2017). Impact of membrane phospholipid alterations in Escherichia coli on cellular function and bacterial stress adaptation. *J. Bacteriol.* **199**, 1–22 http://jb.asm.org/content/199/13/e00849-16.full.pdf%0Ahttp://jb.asm.org/.
25. Hayami, M., Okabe, A., Kariyama, R., Abe, M., Kanemasa, Y., (1979). Lipid composition of staphylococcus aureus and its derived L-forms. *Microbiol. Immunol.* **23**, 435–442. https://doi.org/10.1111/j.1348-0421.1979.tb00483.x.
26. Young, S.A., Desbois, A.P., Coote, P.J., Smith, T.K., (2019). Characterisation of Staphylococcus aureus lipids by nanoelectrospray ionisation tandem mass spectrometry (nESI-MS/MS). *BioRxiv*. https://doi.org/10.1101/593483.
27. Kilelee, E., Pokorny, A., Yeaman, M.R., Bayer, A.S., (2010). Lysyl-phosphatidylglycerol attenuates membrane perturbation rather than surface association of the cationic antimicrobial peptide 6W-RP-1 in a model membrane system: implications for daptomycin resistance. *Antimicrob. Agents Chemother.* **54**, 4476–4479. https://doi.org/10.1128/AAC.00191-10.
28. Hsu, P.C., Samsudin, F., Shearer, J., Khalid, S., (2017). It is complicated: curvature, diffusion, and lipid sorting within the two membranes of *Escherichia coli*. *J. Phys. Chem. Lett.* **8**, 5513–5518. https://doi.org/10.1021/acs.jpclett.7b02432.
29. Gilbert, P., Moore, L.E., (2005). Cationic antiseptics: Diversity of action under a common epithet. *J. Appl. Microbiol.* **99**, 703–715. https://doi.org/10.1111/j.1365-2672.2005.02664.x.
30. Dombek, K.M., Ingram, L.O., (1984). Effects of ethanol on the Escherichia coli plasma membrane. *J. Bacteriol.* **157**, 233–239. https://doi.org/10.1128/jb.157.1.233-239.1984.
31. Ankarloo, J., Wikman, S., Nicholls, I.A., (2010). Escherichia coli mar and acrAB mutants display no tolerance to simple alcohols. *Int. J. Mol. Sci.* **11**, 1403–1412. https://doi.org/10.3390/ijms11041403.
32. Rotter, M.L., (2001). Arguments for alcoholic hand disinfection. *J. Hosp. Infect.* **48**, S4–S8. https://doi.org/10.4324/9780203936313.
33. Rzycki, M., Drabik, D., Szostak-Paluch, K., Hanus-Lorenz, B., Kraszewski, S., (2021). Unraveling the mechanism of octenidine and chlorhexidine on membranes: Does electrostatics matter? *Biophys. J.* **120**, 3392–3408. https://doi.org/10.1016/j.bpj.2021.06.027.
34. Piggot, T.J., Holdbrook, D.A., Khalid, S., (2011). Electroporation of the *E. coli* and *S. aureus* membranes: Molecular dynamics simulations of complex bacterial membranes. *J. Phys. Chem. B* **115**, 13381–13388. https://doi.org/10.1021/jp207013v.
35. Jansson, M., Thurmond, R.L., Trouard, T.P., Brown, M.F., (1990). Magnetic alignment and orientational order of dipalmitoylphosphatidylcholine bilayers containing palmitoyllsyophosphatidylcholine. *Chem. Phys. Lipids* **54**, 157–170.
36. Speyer, J.B., Sripada, P.K., das Gupta, S.K., Shipley, G. G., Griffin, R.G., (1987). Magnetic orientation of sphingomyelin-lecithin bilayers. *Biophys. J.* **51**, 687–691. https://doi.org/10.1016/S0006-3495(87)83394-5.
37. Seelig, J., Borle, F., Cross, T.A., (1985). Magnetic ordering of phospholipid membranes. *Biochim. Biophys. Acta Biomembr.* **814**, 195–198.
38. Ashworth Briggs, E.L., Gomes, R.G.B., Elhussein, M., Collier, W., Stuart Findlow, I., Khalid, S., McCormick, C.J., Williamson, P.T.F., (2015). Interaction between the NS4B amphipathic helix, AH2, and charged lipid headgroups alters membrane morphology and AH2 oligomeric state - Implications for the Hepatitis C virus life cycle. *Biochim. Biophys. Acta Biomembr.* **1848**, 1671–1677. https://doi.org/10.1016/j.bbamem.2015.04.015.
39. Separovic, F. & Sani, M. -A. (2020). Solid State NMR.
40. Feller, S.E., Huster, D., Gawrisch, K., (1999). Interpretation of NOESY cross-relaxation rates from molecular dynamics simulation of a lipid bilayer. *J. Am. Chem. Soc.* **121**, 8963–8964. https://doi.org/10.1021/ja991456n.
41. Kremkow, J., Luck, M., Huster, D., Müller, P., Scheidt, H. A., (2020). Membrane interaction of ibuprofen with cholesterol-containing lipid membranes. *Biomolecules* **10**, 1–12. https://doi.org/10.3390/biom10101384.
42. Holte, L.L., Gawrisch, K., (1997). Determining ethanol distribution in phospholipid multilayers with MAS- NOESY spectra. *Biochemistry* **36**, 4669–4674. https://doi.org/10.1021/bi9626416.
43. Solomon, I., (1955). Relaxation processes in a system of two spins. *Am. Phys. Soc.* **99**, 559.
44. Huster, D., Gawrisch, K., (1988). NOESY NMR Crosspeaks between Lipid Headgroups and Hydrocarbon Chains: Spin Diffusion or Molecular Disorder? *Solid State Nucl. Magn. Reson.* **84**, 95–117. https://doi.org/10.1021/ja.
45. Berglund, N.A., Piggot, T.J., Jefferies, D., Sessions, R.B., Bond, P.J., Khalid, S., (2015). Interaction of the antimicrobial peptide polymyxin B1 with both membranes of *E. coli*: A molecular dynamics study. *PLoS Comput. Biol.* **11** https://doi.org/10.1371/journal.pcbi.1004180.
46. Berendsen, H., Spoel, D., Drunen, R., (1995). GROMACS: A message-passing parallel molecular dynamics implementation. *Comput. Phys. Commun.* **91**, 43–56.
47. Bekker, H., Berendsen, H.J.C., Dijkstra, E.J., Achterop, S., van Drunen, R., van der Spoel, D., Sijbers, A., Keegstra, H., (1993). Gromacs: A parallel computer for molecular dynamics simulations. *Phys. Comput.* **92**, 252–256.
48. Abraham, M.J., Murtola, T., Schulz, R., Páll, S., Smith, J. C., Hess, B., Lindahl, E., (2015). GROMACS: High performance molecular simulations through multi-level parallelism from laptops to supercomputers. *SoftwareX* **1–2**, 19–25.
49. MacKerell Jr, A.D., Bashford, D., Bellott, M.L.D.R., Dunbrack Jr, R.L., Evanseck, J.D., Field, M.J., Fischer, S., Gao, J., et al., (1998). All-atom empirical potential for molecular modeling and dynamics studies of proteins. *J. Phys. Chem. B.* **102**, 3586–3616.
50. Klauda, J.B., Venable, R.M., Freites, J.A., O'Connor, J.W., Tobias, D.J., Mondragon-Ramirez, C., Vorobyov, I., MacKerell Jr, A.D., et al., (2010). Update of the CHARMM all-atom additive force field for lipids: Validation on six lipid types. *J. Phys. Chem. B.* **114**, 7830–7843. https://doi.org/10.1161/CIRCULATIONAHA.110.956839.
51. Nosé, S., (1983). A molecular dynamics method for simulations in the canonical ensemble. *Mol. Phys.* **52**, 255–268.

52. Hoover, W.G., (1985). Canonical dynamics: Equilibrium phase-space distributions. *Phys. Rev. A (Coll Park).* **31**, 1695–1697.
53. Nosé, S., Klein, M.L., (1983). Constant pressure molecular dynamics for molecular systems. *Mol. Phys.* **50**, 1055–1076.
54. Parrinello, M., Rahman, A., (1981). Polymorphic transitions in single crystals: A new molecular dynamics method. *J. Appl. Phys.* **52**, 7182–7190. https://doi.org/10.1063/1.328693.
55. Yu, H., Wang, M.J., Xuan, N.X., Shang, Z.C., Wu, J., (2015). Molecular dynamics simulation of the interactions between EHD1 EH domain and multiple peptides. *J. Zhejiang Univ. Sci. B.* **16**, 883–896. https://doi.org/10.1631/jzus.B1500106.
56. Heumphrey, W., Dalke, A., Schulten, K., (1996). VMD - Visual Molecular Dynamics. *J. Mol. Graph.* **14**, 33–38.
57. van Oosten, B., Marquardt, D., Komljenović, I., Bradshaw, J.P., Sternin, E., Harroun, T.A., (2014). Small molecule interaction with lipid bilayers: A molecular dynamics study of chlorhexidine. *J. Mol. Graph. Model.* **48**, 96–104. https://doi.org/10.1016/j.jmgm.2013.12.007.
58. Jo, S., Kim, T., Iyer, V.G., Im, W., (2008). CHARMM-GUI: A Web-based Graphical User Interface for CHARMM. *J. Comput. Chem.* **29**, 1859–1865.
59. Kluyver, T., Ragan-Kelley, B., Pérez, F., (2016). Jupyter Notebooks – a publishing format for reproducible computational workflows. In: Loizides, F., Schmidt, B. (Eds.), *Positioning and Power in Academic Publishing: Players, Agents and Agendas*. IOS Press, pp. 87–90.
60. Gowers, R.J., Linke, M., Barnoud, J., Reddy, T.J.E., Melo, M.N., Seyler, S.L., Dotson, D.L., Domanski, J., et al., (2016). MDAnalysis: A Python package for the rapid analysis of molecular dynamics simulations. In: Benthall, S., Rostrup, S. (Eds.), *Proceedings of the 15th Python in Science Conference*, pp. 98–105.
61. Hunter, J.D., (2007). Matplotlib: A 2D graphics environment. *Comput. Sci. Eng.* **9**, 90–95.
62. Hahn, E.L., (1950). Spin echoes. *Phys. Rev.* **80**, 580–594. https://doi.org/10.1103/PhysRev.80.580.
63. Jeener, J., Meier, B.H., Bachmann, P., Ernst, R.R., (1979). Investigation of exchange processes by two- dimensional NMR spectroscopy. *J. Chem. Phys.* **71**, 4546–4553. file:///C:/Users/ASUS/Desktop/Rujukan PhD/Dev of drug R cell line/nihms579608.pdf.
64. Marion, D., Ikura, M., Tschudin, R., Bax, A., (1989). Rapid recording of 2D NMR Spectra without phase cycling. Application to the study of hydrogen exchange in proteins. *J. Magn. Reson.* **85**, 393–399.
65. Delaglio, F., Grzesiek, S., Vuister, G.W., Zhu, G., Pfeifer, J., Bax, A., (1995). NMRPipe: a multidimensional spectral processing system based on UNIX pipes. *J. Biol. NMR.* **6**, 277–293.
66. MATLAB (2021). MATLAB and Statistics Toolbox Release R2021a.
67. van Beek, J.D., (2007). matNMR: A flexible toolbox for processing, analyzing and visualizing magnetic resonance data in Matlab®. *J. Magn. Reson.* **187**, 19–26. https://doi.org/10.1016/j.jmr.2007.03.017.
68. Skinner, S.P., Fogh, R.H., Boucher, W., Ragan, T.J., Mureddu, L.G., Vuister, G.W., (2016). CcpNmr AnalysisAssign: a flexible platform for integrated NMR analysis. *J. Biomol. NMR* **66**, 111–124. https://doi.org/10.1007/s10858-016-0060-y.